



# Integrated molecular and clinical analysis of low-grade gliomas in children with neurofibromatosis type 1 (NF1)

Michael J. Fisher<sup>1</sup> · David T. W. Jones<sup>2,3</sup> · Yimei Li<sup>4</sup> · Xiaofan Guo<sup>5</sup> · Poonam S. Sonawane<sup>6</sup> · Angela J. Waanders<sup>1,23</sup> · Joanna J. Phillips<sup>7</sup> · William A. Weiss<sup>8</sup> · Adam C. Resnick<sup>6</sup> · Sara Gosline<sup>9,24</sup> · Jineta Banerjee<sup>9</sup> · Justin Guinney<sup>9</sup> · Astrid Gnekow<sup>10</sup> · Daniela Kandels<sup>10</sup> · Nicholas K. Foreman<sup>11</sup> · Andrey Korshunov<sup>12</sup> · Marina Ryzhova<sup>13</sup> · Luca Massimi<sup>14,28</sup> · Sri Gururangan<sup>15</sup> · Mark W. Kieran<sup>16,25</sup> · Zhihong Wang<sup>17,26</sup> · Maryam Fouladi<sup>18,27</sup> · Mariko Sato<sup>19</sup> · Ingrid Øra<sup>20</sup> · Stefan Holm<sup>21</sup> · Stephen J. Markham<sup>1</sup> · Pengbo Beck<sup>2,3</sup> · Natalie Jäger<sup>2,3</sup> · Andrea Wittmann<sup>2</sup> · Alexander C. Sommerkamp<sup>2,3</sup> · Felix Sahn<sup>12</sup> · Stefan M. Pfister<sup>2,3,22</sup> · David H. Gutmann<sup>5</sup>

Received: 18 December 2020 / Revised: 21 January 2021 / Accepted: 22 January 2021 / Published online: 14 February 2021  
© The Author(s), under exclusive licence to Springer-Verlag GmbH, DE part of Springer Nature 2021

## Abstract

Low-grade gliomas (LGGs) are the most common childhood brain tumor in the general population and in individuals with the Neurofibromatosis type 1 (NF1) cancer predisposition syndrome. Surgical biopsy is rarely performed prior to treatment in the setting of NF1, resulting in a paucity of tumor genomic information. To define the molecular landscape of NF1-associated LGGs (NF1-LGG), we integrated clinical data, histological diagnoses, and multi-level genetic/genomic analyses on 70 individuals from 25 centers worldwide. Whereas, most tumors harbored bi-allelic *NF1* inactivation as the only genetic abnormality, 11% had additional mutations. Moreover, tumors classified as non-pilocytic astrocytoma based on DNA methylation analysis were significantly more likely to harbor these additional mutations. The most common secondary alteration was *FGFR1* mutation, which conferred an additional growth advantage in multiple complementary experimental murine *Nf1* models. Taken together, this comprehensive characterization has important implications for the management of children with NF1-LGG, distinct from their sporadic counterparts.

**Keywords** Pilocytic astrocytoma · Pediatric brain tumor · Neurofibromatosis · Methylation · FGFR1

## Introduction

Children with the Neurofibromatosis type 1 (NF1) cancer predisposition syndrome are at significantly elevated risk for the development of brain tumors, particularly low-grade gliomas (LGGs) [9]. These tumors most typically arise within the optic pathway/hypothalamus (66–75%), followed by the brainstem (10–15%) [16], where progressive vision loss or other neurologic signs and symptoms, respectively, prompt the need for chemotherapy. NF1-LGGs arising outside of

these locations more often exhibit continued growth, which may necessitate repetitive therapeutic interventions, including multiple different chemotherapy regimens [17]. These tumors are rarely surgically resected or biopsied, and most are presumed to be pilocytic astrocytoma (World Health Organization grade I). As such, pathological confirmation is not an element of current management planning [19]. In an effort to establish the molecular landscape of pediatric NF1-LGGs relevant to clinical management, we performed the largest and most comprehensive analysis of molecularly and clinically annotated low-grade gliomas arising in children and adolescents with NF1 to date.

---

Michael J. Fisher and David T. W. Jones are co-first authors.

---

Stefan M. Pfister and David H. Gutmann are co-last authors.

---

✉ Michael J. Fisher  
fisherm@chop.edu

✉ David H. Gutmann  
gutmann@wustl.edu

Extended author information available on the last page of the article

## Materials and methods

### Study population, IRB approval, and data abstracted

Tumor specimens from children and adolescents (< 19 years of age) with NF1, who underwent biopsy or surgical resection of their tumor as part of medically-indicated clinical management, and had a histological diagnosis of LGG were included in accordance with local institutional IRB guidelines (Supplemental methods, online resource). A diagnosis of NF1 was established using NIH Consensus Conference clinical diagnostic criteria [18]. Available tumor specimens with matched germline DNA (or blood or saliva) when available were submitted to the German Cancer Research Center (DKFZ) in Heidelberg for comprehensive genomic analyses. Clinical data, including age at biopsy, sex, race/ethnicity, NF1 inheritance, tumor location and histology, reason for biopsy, other treatment information, and age/status at last follow-up, were abstracted from existing clinical records for each subject. No personal health information was abstracted.

### Sample processing

Sample processing including DNA and RNA extraction and quality controls (tumor cell content, histopathological assessment, quantification and quality of analytes) were performed as previously described [24, 30] using standard protocols.

### Whole-genome sequencing (WGS) and RNA sequencing

31 matched tumor-normal pairs were profiled with whole-genome sequencing (WGS; median 79.6-fold coverage for tumor and 77.6-fold for normal, with range 72.9–86.0× and 71.6–85.4×, respectively) using an Illumina HiSeqX. Whole transcriptome data (RNAseq) were generated for 33 samples using a strand-specific, polyA-enriched library protocol, with a median of 193.4 million mapped reads per sample (range 94.0–262.7 million). Sequencing coverage statistics are provided in Supplementary Table 1 (online resource). WGS libraries were prepared using the Illumina TruSeq Nano kit and sequenced on Illumina HiSeq X Ten V2.5 in paired-end mode. RNAseq libraries were prepared using a strand-specific, polyA-enriched library protocol (Illumina TruSeq kit) and sequenced on the Illumina HiSeq 4000 in paired-end mode. All samples were only included for library preparation after passing all standard quality controls. One further case (SYN\_NF\_092) was profiled with whole-exome and low-coverage whole-genome sequencing in addition to RNA sequencing through the INFORM personalized

medicine platform [31]. Matched tumor and blood samples from 9 samples were assessed using a targeted gene panel approach [23].

### Alignment of WGS data

Alignments were performed according to the standards defined for ICGC PanCancer [24]. All reads were aligned against the phase II reference of the 1000 Genomes Project including decoy sequences d5 ([ftp://ftp.1000genomes.ebi.ac.uk/vol1/ftp/technical/reference/phase2\\_reference\\_assembly\\_sequence/hs37d5.fa.gz](ftp://ftp.1000genomes.ebi.ac.uk/vol1/ftp/technical/reference/phase2_reference_assembly_sequence/hs37d5.fa.gz)) using BWA MEM (v.0.7.15 using standard values except for invoking -T 0) [14]. The raw BAM files were sorted and duplicates were marked using sambamba (SAMBAMBA MARKDUP\_VERSION=0.6.5). Sequencing coverage was calculated using custom scripts [11].

### Mutation calling of SNVs and indels

Detection of somatic and germline SNVs and insertions or deletions (indels) in the WGS data was performed using the DKFZ in-house pipeline “Roddy”. The pipeline is based on SAMtools (v.0.1.19) mpileup and bcftools using parameter adjustments allowing for SNV calling even with low allele frequency in the tumor [11]. In short, variants were first called in the tumor sample and then queried in the matching control sample. The raw calls were subsequently annotated using multiple publicly available tracks, such as 1000 Genome variants, single-nucleotide polymorphism database (dbSNP), repeats and other elements. The functional effect of the mutations was annotated using Annovar [28] and the variants were assessed for their confidence (based in read depth, sequence context, and many more parameters) and split into somatic and germline calls. SNVCallingWorkflow:1.2.166–1 was used in this project. The small insertion/deletion (indel) detection workflow is based on Platypus [23] with extensive quality control additions for the DKFZ developed workflow management system “Roddy”. Indel-CallingWorkflow:1.2.177 was used in this project.

### Allele-specific copy number estimation with whole-genome sequencing (ACEseq)

ACEseq estimates allele-specific copy numbers from WGS data (<https://www.biorxiv.org/content/10.1101/210807v1.full>) using both a coverage ratio of tumor and control over genome windows and the B-allele frequency (BAF), producing copy number calls and estimates of tumor ploidy and cell content. ACEseqWorkflow:1.2.8–3 was used in this project.

## RNAseq analysis

The STAR aligner [5] was used for alignment (version 2.5.3a). Reads were aligned to a STAR index generated from the 1000 genomes assembly, gencode 19 gene models and for *asjbdOverhang* of 200. The tool Featurecounts [15] was used to perform gene-specific read counting over exon features based on the gencode 19 gene models. Both reads of a paired fragment were used for counting and the quality threshold was set to 255 (which indicates that STAR found a unique alignment). Strand unspecific counting was used. A custom script was used to calculate RPKM and TPM expression values. For total library abundance calculations, all genes on chromosomes X, Y, MT and rRNA and tRNA genes were omitted as they are likely to introduce library size estimation biases. Gene fusions were identified using the *arriba* algorithm (version 0.8, <https://github.com/suhri/arriba/>). RNAseqWorkflow: 1.3.0 was used in this project.

## Prediction of tumor-infiltrating immune cell fraction

The amounts of immune and stromal infiltration in the tumor samples were inferred by ESTIMATE (Estimation of STromal and Immune cells in MAlignant Tumor tissues using Expression data) [32].

## DNA methylation analysis

Genome-wide DNA methylation analysis was performed and processed using the Illumina HumanMethylation450 (450 k) or HumanMethylationEPIC BeadChip array [3]. Further processing and genome-wide copy number analyses were performed using the ‘conumee’ package in R (<http://bioconductor.org/packages/release/bioc/html/conumee.html>).

## NIH3T3 cell analyses

*Nf1* knockdown was achieved by CRISPR/CAS9 engineering in NIH-3T3 cells using *Nf1* targeted gRNA Santa Cruz (sc-421861), and single positive clones sorted for green fluorescence protein expression using FACS/Jazz. Gateway cloning was used to transduce cells with vector control or mutant *FGFR*<sup>N546K</sup>. Cell transformation by anchorage-independent growth (soft agar assay) was quantitated using relative fluorescence units (RFU), measured using the CytoSelect 96-Well Cell Transformation Assay (Cell Biolabs).

## Murine glioma analysis

Murine optic glioma stem cells lacking *Nf1* expression (o-GSCs) were virally transduced with mutant human *FGFR* (N546K, K656E), and expression verified by Western blotting [4]. Cell growth was assessed by direct cell

counting in vitro, while glioma-like formation determined 6 months following the injection of  $5 \times 10^5$  empty vector or *FGFR*-K656E-expressing o-GSCs into the brainstems of wild-type mice, and assessed by Ki67 indices in vivo [4, 20]. At least five samples per group were analyzed, with statistical significance set at  $P < 0.05$  using the Student's *t* test.

## Western blot

Phospho-MEK<sup>Ser217/221</sup> (#9154), MEK (#4694), phospho-ERK<sup>Thr202/Tyr204</sup> (#4370), ERK (#4695), phospho-AKT<sup>Ser473</sup> (#4060), phospho-AKT<sup>Thr308</sup> (#4056), AKT (#2920), phospho-S6<sup>Ser240/244</sup> (#2215),  $\beta$ -actin (#4125), Myc-Tag (#2040S), and S6 (#2317) antibodies were purchased from Cell Signaling, while *FGFR1* (ab76464), neurofibromin (ab17963), and  $\alpha$ -tubulin (ab176560) antibodies were purchased from Abcam. Development using secondary antibodies was performed as previously reported [4].

## Statistical analyses

Patient clinical characteristics were summarized using descriptive statistics, such as mean, median and range for continuous variables, and frequency and percent for categorical variables. Distribution of the characteristics was also summarized by tumor location or by methylation status, and the differences across tumor location (or methylation status) were compared using Kruskal–Wallis test for continuous variables and Fisher's exact for categorical variables. The analyses were performed in SAS 9.3 and a two-sided *P* value of  $< 0.05$  was considered statistically significant.

## Data availability

Raw sequencing data were deposited in SAGE (<https://doi.org/10.7303/syn5698493>).

## Results

### Spectrum of *NF1* alterations

The cohort with molecular data includes 70 *NF1*-LGG specimens from 70 individuals with a confirmed diagnosis of *NF1* under the age of 19 years. These specimens were collected from 25 different medical centers throughout the world. Clinical annotation was available for 48 subjects (Table 1), whereas only limited clinical data could be collected for the other 22 subjects. Multiple platforms were used for genomic characterization (Supplementary Table 2, online resource). 31 matched tumor-normal pairs were profiled with whole-genome sequencing (WGS), while whole transcriptome data (RNAseq) were generated for 33 samples.

**Table 1** Demographics of clinical cohort

Age at biopsy (years)	
Mean	9.6
Median (range)	9.5 (1.9–18.9)
Length of follow-up (years)	
Mean	4.1
Median (range)	3.9 (0.1–19.3)
Clinical variable	Number (%)
<b>Sex</b>	
Female	23 (48%)
Male	25 (52%)
<b>Race/ethnicity</b>	
White/non-hispanic or latino	35 (73%)
White/hispanic or latino	4 (8%)
Other/non-hispanic or latino	3 (6%)
Unknown	6 (12%)
<b>NF1 inheritance</b>	
Familial	13 (27%)
Sporadic	24 (50%)
Unknown	11 (23%)
<b>Clinical status</b>	
Alive	43 (90%)
Deceased	1 (2%)
Lost to follow-up	4 (8%)
<b>Biopsy site</b>	
Cortex	17 (35%)
OPHG	13 (27%)
Cerebellar/PF NOS	10 (21%)
Brainstem	4 (8%)
Midline	3 (6%)
Ventricle	1 (2%)
<b>Treatment</b>	
No	19 (40%)
Chemo	25 (52%)
Unknown	4 (8%)
<b>Histology</b>	
LGG—PA	28 (58%)
LGG—PA (PMA)	3 (6%)
LGG—PA with atypical features	3 (6%)
LGG—Grade 2 (DA)	5 (10%)
LGG—Grade 2 (OA)	1 (2%)
LGG—Grade 2 (PXA)	1 (2%)
LGG—NOS	6 (13%)
Brain Tumor—NOS	1 (2%)
<b>Methylation subtype</b>	
PA	39 (81%)
APA	1 (2%)
LGGNT	2 (4%)
MYB	2 (4%)
RGNT	1 (2%)

**Table 1** (continued)

Clinical variable	Number (%)
N/A	3 (6%)
Has other mutation	
No	43 (90%)
Yes	5 (10%)

APA anaplastic pilocytic astrocytoma, DA diffuse astrocytoma, LGG low-grade glioma, LGGNT low-grade glioma and glioneuronal tumor, MYB MYB methylation group, N/A not available, NOS not otherwise specified, OA oligoastrocytoma, OPHG optic pathway/hypothalamic glioma, PA pilocytic astrocytoma, PF posterior fossa, PMA pilomyxoid astrocytoma, PXA pleomorphic xanthoastrocytoma, RGNT rosette-forming glioneuronal tumor

In addition, a targeted gene panel sequencing approach was used for 9 subjects with matched tumor and blood samples. Genome-wide DNA methylation analysis was performed on 67 tumors.

Whole-genome sequencing analysis confirmed a generally low mutation rate across the cohort, as expected for low-grade pediatric tumors [8]. On average, we detected only 6 non-synonymous somatic single-nucleotide mutations per tumor (range 0–22), and 1 small insertion/deletion (indel; range 0–2). The germline *NF1* alteration was detected in 30/31 (97%) of the WGS tumors, demonstrating the high sensitivity of this method for genetic confirmation of *NF1* mutations. The one case with no apparent germline alteration displayed a copy-neutral LOH of chromosome 17q, together with a frameshift indel in the tumor; somatic mosaicism for the indel cannot be excluded. For the cases with targeted gene panel analysis, the germline *NF1* alteration was identified in 7/9 cases (78%), perhaps owing to the inferior sensitivity of the panel sequencing approach to detect certain classes of alterations, such as deeper intronic mutations, large deletions or those in regions poorly captured in the target enrichment.

In 27 of 31 tumors with WGS data (87%), we could identify the somatic *NF1* alteration, thus confirming the typical pattern of bi-allelic inactivation reported for NF1-LGG [10] (Fig. 1). All but one of the tumors belonging to the PA molecular class by methylation analysis (23/24 samples) demonstrated this two-hit pattern of *NF1* inactivation. The one exception (SYN\_NF\_043) was found to harbor very low tumor cell content in the tissue analyzed, and the second hit may have been missed despite the high sequencing depth. Notably, all of the identified somatic *NF1* mutations (i.e., non-LOH cases) were truncating (either stopgain or frameshift).

While the somatic *NF1* mutations were scattered throughout the coding region, there was a modest 5' bias for germline *NF1* gene mutations ( $n = 15$ ,  $n = 14$  and  $n = 4$  mutations in the first, second and third tertile of the coding region, respectively), which was not significantly different from the distribution observed in a cohort of NF1 patients without glioma ( $P = 0.42$ ; Chi-square test) [1]. Four further

cases showed a large deletion including *NF1*, and one was uninformative; Fig. 1).

### Secondary molecular alterations and functional assessment of *FGFR1* mutation in *Nf1*-deficient cells

In addition to the *NF1* mutation, five tumors with WGS/WES data harbored a further alteration considered to be 'glioma-relevant', and thus a likely co-driver event. These mutually exclusive events included *FGFR1* mutation ( $n = 3$ , two also with additional *PIK3CA* mutations), *MYB:QKI* fusion ( $n = 1$ ), and a *SETD2* mutation ( $n = 1$ ) (Fig. 2a, b). The *MYB:QKI* fusion was also detected in targeted gene fusion analysis [13]. Targeted gene panel sequencing, performed in 9 samples, did not identify any additional non-*NF1* mutations.

Since *FGFR1* was found to be recurrently mutated, similar to sporadic PA [12], we sought to determine the functional significance of this co-occurring mutation using several complementary assays. First, we showed that both NF1 wild-type (WT) CRISPR-engineered *Nf1*-deficient murine (*Nf1*-null) NIH3T3 cells expressing the *FGFR1* N546K mutation exhibit increased MEK/ERK pathway activation and increased numbers of colonies relative to their respective controls (Fig. 3a). Second, we leveraged *Nf1*-deficient low-grade glioma cells derived from 3-month-old *Nf1*-mutant mice with optic glioma [4] to demonstrate that ectopic expression of mutant human *FGFR1* (N546K, K565E) increased tumor cell growth and MEK/ERK activation in vitro (Fig. 3b). Third, we took advantage of the fact that these *Nf1*-deficient mouse optic glioma stem cells (o-GSCs) can form tumors following transplantation into immunocompetent mice [4]. We specifically injected o-GSCs using cell concentrations ( $5 \times 10^5$  cells in 2  $\mu$ l) where tumors do not form in wild-type mice. Transplantation of one of these *FGFR1*-mutant *Nf1*-deficient o-GSC lines into the brainstems of wild-type mice revealed tumors in 4/5 mice injected, compared to 0/5 mice receiving only *Nf1*-deficient o-GSCs (Fig. 3c). Together, these data establish a clear functional consequence of *FGFR1* mutation in combination with *Nf1* loss on LGG biology.

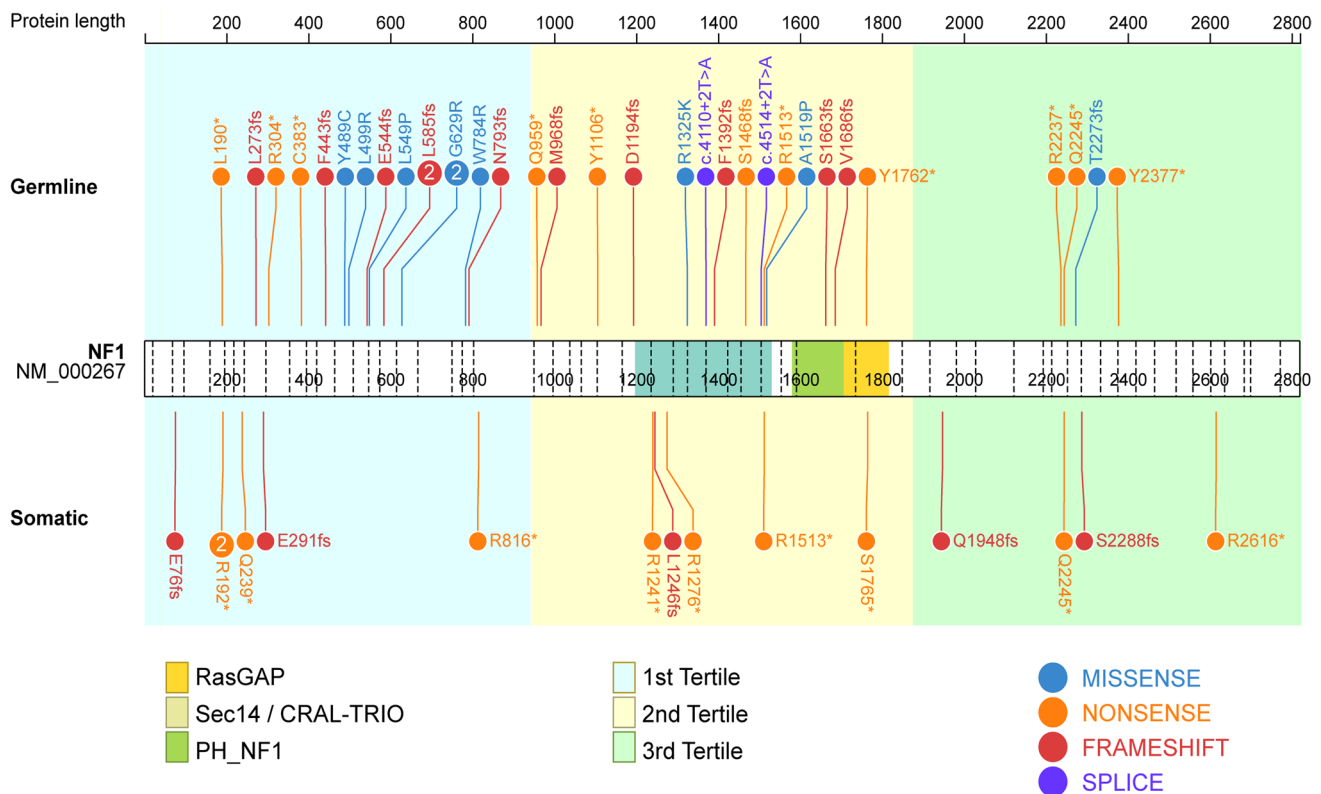


**Fig. 1** Lollipop plot demonstrating the position and frequency of germline (top) and somatic (bottom) *NF1* gene mutations in 31 tumors from children with NF1 with WGS data

## Methylation analysis

Next, we sought to investigate the spectrum of molecular tumor classes represented by the *NF1*-associated tumors by comparing their global DNA methylation patterns to a reference cohort of other known classes of glial and glioneuronal tumors using a t-SNE visualization and the Molecular Neuropathology brain tumor classifier ([www.molecularneuropathology.org/mnp](http://www.molecularneuropathology.org/mnp); [3]) (Fig. 2c). One tumor (SYN\_NF\_088) could not be reliably characterized due to a low tumor cell content in the analyzed tissue. As expected, the majority of the remaining tumors (58/66, 88%) displayed a strong similarity to sporadic PA from varying anatomic locations (posterior fossa, midline, hemispheric).

Two tumors resembled low-grade glial/glioneuronal tumors without further specification possible, while two had a methylation profile matching that of rosette-forming glioneuronal tumors (RGNTs, see below). Unexpectedly, two of the pediatric *NF1*-associated tumors (including the one with the *MYB:QKI* alteration) showed a DNA methylation profile resembling that of *MYB/MYBL1*-altered glioma, which is most often associated with angiocentric or isomorphic diffuse gliomas [2, 21, 29]. In addition, there were two tumors, histologically diagnosed as low-grade, which

displayed a methylation pattern more fitting of high-grade astrocytoma with piloid features (HGAP, also referred to as APA, anaplastic PA or anaplastic astrocytoma with piloid features) and harbored a homozygous deletion of the 9p21 locus (including *CDKN2A/B*)—a hallmark genetic lesion of this entity [22] (Supplementary Fig. 1, online resource). The copy number profile of most of the other tumors was relatively quiet, with only broad whole chromosome gains, as often seen in sporadic PAs [6]. Of note, there were two individuals for which specimens were submitted for two separate surgeries on the same tumor, one with an interval of three years between surgeries, the other with an eight-year gap between surgeries. In both cases, there were no differences in methylation group or somatic mutations between the samples.

## Transcriptional analysis

At the global transcriptomic level, *NF1* expression was lower in the *NF1*-associated tumors, as expected (Fig. 4a). Consistent with the established function of the *NF1* protein (neurofibromin) as a negative RAS/RAS pathway regulator, the median MAPK pathway activation score (MPAS)

was elevated [27], similar to that observed in sporadic *KIAA1549:BRAF*-driven PAs [26] (Fig. 4b).

In addition, based on studies in both *Nf1* murine experimental LGG models and human NF1-PAs, a significant proportion of the cellular content of these tumors was composed of non-neoplastic cells, including microglia/macrophages. To assess the stromal composition, we applied the ESTIMATE algorithm to judge the overall immune content [32]. While the degree of stromal infiltration into the tumor, as assessed by transcript expression profiles calculated using the ESTIMATE algorithm, was relatively low [167 (–268 to 602), mean ( $\pm$  SD)], the degree of immune infiltration was much higher [1448 (728–2169), mean ( $\pm$  SD)] (Fig. 4c).

### Integrated clinical and molecular analysis

48 subjects had clinical information in addition to their molecular analyses (Table 1). The median length of follow-up was 3.9 years (range 0.1–19.3 years). There was no sex predilection, and 81% of the cohort was Caucasian. The most common locations for these biopsied tumors were the cortex (35%), optic pathway/hypothalamus (27%), and cerebellum (21%), which likely reflects the clinical decision to biopsy tumors outside of the optic pathway/hypothalamus or those with unusual growth characteristics. As expected by the known younger age of optic pathway/hypothalamic glioma (OPHG) presentation (4.5 years), the median age at biopsy was 2.8 years for subjects with OPHG tumors compared to 7.8–11.7 years for subjects with tumors in other locations ( $P=0.02$ ; Table 2). Histopathologic analysis revealed that 70% of tumors were PAs or PA variants (e.g., pilomyxoid).

Combining the clinical and molecular findings, we found that the histologic assessment did not always match the methylation group assignment (Supplementary Table 3, online resource). As such, 88% of the tumors in the entire cohort and 87% of those in the core clinical cohort were classified as PA by methylation—slightly higher than the fraction based on histology (56% classical PA; 64% including PA variants in the entire cohort). In addition, tumors of non-PA methylation classes were more likely to harbor an additional non-*NF1* mutation (3/4 vs 1/24 cases with methylation and WGS data in non-PA and PA methylation classes, respectively;  $P=0.005$ , Fisher's exact test). When WES and targeted gene panel sequencing data on an additional 10 specimens are included, this difference in finding an additional non-*NF1* mutation remains significant (3/5 vs. 2/33 cases in non-PA and PA methylation classes, respectively;  $P=0.011$ , Fisher's exact test). Only 7.7% of OPHGs harbored other mutations or were not classified by methylation as a PA, compared with 20.6% of those arising elsewhere; however, this difference was not significant ( $P=0.41$ ). In contrast, there was no difference between patients, based on age, for the presence of an additional non-*NF1* mutation

or non-PA methylation class, whether ages were divided in halves (age < 10 versus age 10 to < 19 years) (Supplementary Table 4, online resource) or thirds (age < 6.5, between 6.5 and < 13, or between 13 and < 19 years) (Supplementary Table 5, online resource). Of those with survival data, there was only one death, which occurred in a patient with a brainstem APA (by methylation) biopsied at 11 years of age. Although the overall survival for the cohort was 98%, 52% of children required chemotherapy either before or after biopsy, of which over half required more than one chemotherapeutic regimen.

### Discussion

The present study has potential inherent biases and limitations, including the inclusion of subjects from tertiary specialty referral centers, differences in the clinical indications for biopsy, the inclusion of children whose tumors were potentially biopsied due to unusual behavior, and restrictions on the amount and type of material available for molecular characterization. Despite this, the findings from this largest molecular study of an NF1-LGG population raise several important points. *First*, the vast majority of pediatric NF1-brain tumors were PAs (> 85%). *Second*, an unexpected number (7/38; 18.4%) of samples with both DNA and methylation data were classified as a non-PA and/or harbored an additional non-*NF1* mutation. *Third*, tumors arising in the optic pathway or hypothalamus were unlikely to harbor other mutations or be classified by methylation as something other than PA. However, the small sample size does not allow us to determine definitively whether tumors from different locations preferentially harbor other mutations or would be classified as non-PA. Power calculations reveal that a total sample size of 226 would be required to achieve 80% power to detect the observed difference at the 0.05 significance level. For this reason, the impact of tumor location is unlikely to be elucidated in the near future. *Fourth*, while the germline *NF1* gene abnormality could be found in all five cases with WGS/WES and germline data in which additional non-*NF1* genetic/genomic alterations were identified, a somatic abnormality in the second *NF1* allele was not found in 3 samples (two with *FGFR1 + PIK3CA* mutations, one with a *MYB:QKI* alteration). This suggests that in rare cases, glioma pathogenesis in the context of NF1 may not depend on loss of the second *NF1* allele, as reported for a young adult with NF1 and a malignant glioma [30]. *Fifth*, although concerns have been raised in the NF community about an increased risk of more aggressive tumor behavior in teenage patients (high grade or APA methylation groups), if the tumor is a LGG by histology, our results indicate that there is not an increased risk of finding an additional mutation or non-PA methylation class in this age group. *Sixth*,

**a**

Sample ID	Location	Histo Dx	Methylation Group	Germline NF1	Somatic NF1	Additional hits
SYN_NF_004	Cereb.	PA	PA			
SYN_NF_007	Cereb.	PA	PA			
SYN_NF_009	Brainstem	PA	PA			
SYN_NF_012	Post.Fosa	PA	PA			
SYN_NF_034	Cereb.	DA	PA			
SYN_NF_037	Post.Fosa	RGNT	RGNT			<i>FGFR1-4pN3CA</i>
SYN_NF_038	Cereb.	PA	PA			
SYN_NF_048	Cereb.	PA	PA			
SYN_NF_055	OPHG	PA	PA			
SYN_NF_057	OPHG	PA	PA			<i>S.FDZ3-stopgap</i>
SYN_NF_058	Brainstem	PA	PA			
SYN_NF_059	Post.Fosa	PA	PA			
SYN_NF_066	OPHG	PA	PA			
SYN_NF_070	Cereb.	PA	LOG_MYB			<i>GR7.MYB</i>
SYN_NF_073	Cereb.	PA	LOG_MYB			
SYN_NF_074	Cereb.	PA	LOG_MYB			
SYN_NF_075	Cereb.	PA	LOG_MYB			
SYN_NF_076	Cereb.	PA	LOG_MYB			
SYN_NF_077	Cereb.	PA	LOG_MYB			
SYN_NF_078	Cereb.	PA	LOG_MYB			
SYN_NF_079	Cereb.	PA	LOG_MYB			
SYN_NF_080	Cereb.	PA	LOG_MYB			
SYN_NF_081	Cereb.	PA	LOG_MYB			
SYN_NF_082	Cereb.	PA	LOG_MYB			
SYN_NF_083	Cereb.	PA	LOG_MYB			
SYN_NF_084	Cereb.	PA	LOG_MYB			
SYN_NF_085	Cereb.	PA	LOG_MYB			
SYN_NF_086	Cereb.	PA	LOG_MYB			
SYN_NF_087	Cereb.	PA	LOG_MYB			
SYN_NF_088	Cereb.	PA	LOG_MYB			
SYN_NF_089	Cereb.	PA	LOG_MYB			
SYN_NF_090	Cereb.	PA	LOG_MYB			
SYN_NF_091	Cereb.	PA	LOG_MYB			
SYN_NF_092	Cereb.	PA	LOG_MYB			
SYN_NF_093	Cereb.	PA	LOG_MYB			
SYN_NF_094	Cereb.	PA	LOG_MYB			
SYN_NF_095	Cereb.	PA	LOG_MYB			
SYN_NF_096	Cereb.	PA	LOG_MYB			
SYN_NF_097	Cereb.	PA	LOG_MYB			
SYN_NF_098	Cereb.	PA	LOG_MYB			
SYN_NF_099	Cereb.	PA	LOG_MYB			
SYN_NF_100	Cereb.	PA	LOG_MYB			
SYN_NF_101	Cereb.	PA	LOG_MYB			
SYN_NF_102	Cereb.	PA	LOG_MYB			
SYN_NF_103	Cereb.	PA	LOG_MYB			
SYN_NF_104	Cereb.	PA	LOG_MYB			
SYN_NF_105	Cereb.	PA	LOG_MYB			
SYN_NF_106	Cereb.	PA	LOG_MYB			
SYN_NF_107	Cereb.	PA	LOG_MYB			
SYN_NF_108	Cereb.	PA	LOG_MYB			
SYN_NF_109	Cereb.	PA	LOG_MYB			
SYN_NF_110	Cereb.	PA	LOG_MYB			
SYN_NF_111	Cereb.	PA	LOG_MYB			
SYN_NF_112	Cereb.	PA	LOG_MYB			
SYN_NF_113	Cereb.	PA	LOG_MYB			
SYN_NF_114	Cereb.	PA	LOG_MYB			
SYN_NF_115	Cereb.	PA	LOG_MYB			
SYN_NF_116	Cereb.	PA	LOG_MYB			
SYN_NF_117	Cereb.	PA	LOG_MYB			
SYN_NF_118	Cereb.	PA	LOG_MYB			
SYN_NF_119	Cereb.	PA	LOG_MYB			
SYN_NF_120	Cereb.	PA	LOG_MYB			
SYN_NF_121	Cereb.	PA	LOG_MYB			
SYN_NF_122	Cereb.	PA	LOG_MYB			
SYN_NF_123	Cereb.	PA	LOG_MYB			
SYN_NF_124	Cereb.	PA	LOG_MYB			
SYN_NF_125	Cereb.	PA	LOG_MYB			
SYN_NF_126	Cereb.	PA	LOG_MYB			
SYN_NF_127	Cereb.	PA	LOG_MYB			
SYN_NF_128	Cereb.	PA	LOG_MYB			
SYN_NF_129	Cereb.	PA	LOG_MYB			
SYN_NF_130	Cereb.	PA	LOG_MYB			
SYN_NF_131	Cereb.	PA	LOG_MYB			
SYN_NF_132	Cereb.	PA	LOG_MYB			
SYN_NF_133	Cereb.	PA	LOG_MYB			
SYN_NF_134	Cereb.	PA	LOG_MYB			
SYN_NF_135	Cereb.	PA	LOG_MYB			
SYN_NF_136	Cereb.	PA	LOG_MYB			
SYN_NF_137	Cereb.	PA	LOG_MYB			
SYN_NF_138	Cereb.	PA	LOG_MYB			
SYN_NF_139	Cereb.	PA	LOG_MYB			
SYN_NF_140	Cereb.	PA	LOG_MYB			
SYN_NF_141	Cereb.	PA	LOG_MYB			
SYN_NF_142	Cereb.	PA	LOG_MYB			
SYN_NF_143	Cereb.	PA	LOG_MYB			
SYN_NF_144	Cereb.	PA	LOG_MYB			
SYN_NF_145	Cereb.	PA	LOG_MYB			
SYN_NF_146	Cereb.	PA	LOG_MYB			
SYN_NF_147	Cereb.	PA	LOG_MYB			
SYN_NF_148	Cereb.	PA	LOG_MYB			
SYN_NF_149	Cereb.	PA	LOG_MYB			
SYN_NF_150	Cereb.	PA	LOG_MYB			
SYN_NF_151	Cereb.	PA	LOG_MYB			
SYN_NF_152	Cereb.	PA	LOG_MYB			
SYN_NF_153	Cereb.	PA	LOG_MYB			
SYN_NF_154	Cereb.	PA	LOG_MYB			
SYN_NF_155	Cereb.	PA	LOG_MYB			
SYN_NF_156	Cereb.	PA	LOG_MYB			
SYN_NF_157	Cereb.	PA	LOG_MYB			
SYN_NF_158	Cereb.	PA	LOG_MYB			
SYN_NF_159	Cereb.	PA	LOG_MYB			
SYN_NF_160	Cereb.	PA	LOG_MYB			
SYN_NF_161	Cereb.	PA	LOG_MYB			
SYN_NF_162	Cereb.	PA	LOG_MYB			
SYN_NF_163	Cereb.	PA	LOG_MYB			
SYN_NF_164	Cereb.	PA	LOG_MYB			
SYN_NF_165	Cereb.	PA	LOG_MYB			
SYN_NF_166	Cereb.	PA	LOG_MYB			
SYN_NF_167	Cereb.	PA	LOG_MYB			
SYN_NF_168	Cereb.	PA	LOG_MYB			
SYN_NF_169	Cereb.	PA	LOG_MYB			
SYN_NF_170	Cereb.	PA	LOG_MYB			

**b**

Sample ID	Location	Histo Dx	Methylation Group	Germline NF1	Somatic NF1	Additional hits
SYN_NF_062	PA	PA	PA			
SYN_NF_113	RGNT	RGNT	RGNT			<i>FGFR1 + PIK3CA</i>
SYN_NF_115	LGG -NOS	LGG -NOS	PA			
SYN_NF_118	LGG -NOS	LGG -NOS	PA			
SYN_NF_172	PA	PA	PA			
SYN_NF_174	PA	PA	PA			
SYN_NF_060	PA	PA	PA			
SYN_NF_061	PA	PA	PA			
SYN_NF_084	PA	LGG -NOS	PA			
SYN_NF_086	PA	LGG -NOS	PA			
SYN_NF_087	PA	PXA	PA			
SYN_NF_173	PA	PA	PA			
SYN_NF_035	PA	LGG -NOS	PA			
SYN_NF_080	PA	LGG -NOS	HGAP			<i>9p21 del/PIK3RA amp</i>
SYN_NF_114	PA	LGG -NOS	PA			
SYN_NF_117	PA	LGG -NOS	PA			
SYN_NF_083	PA	PA	PA			
SYN_NF_064	PA	LGG -NOS	PA			
SYN_NF_088	PA	LGG -NOS	PA			<i>EGFR amp</i>
SYN_NF_093	PA	PA	PA			
SYN_NF_168	PA	PA	PA			
SYN_NF_171	PA	PA	PA			

**c**

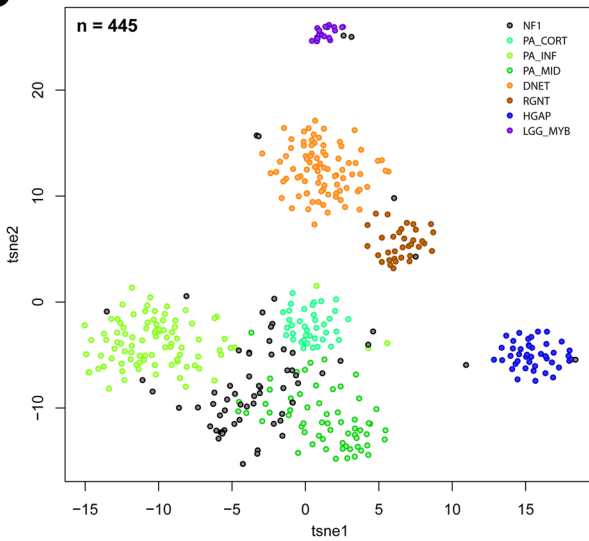
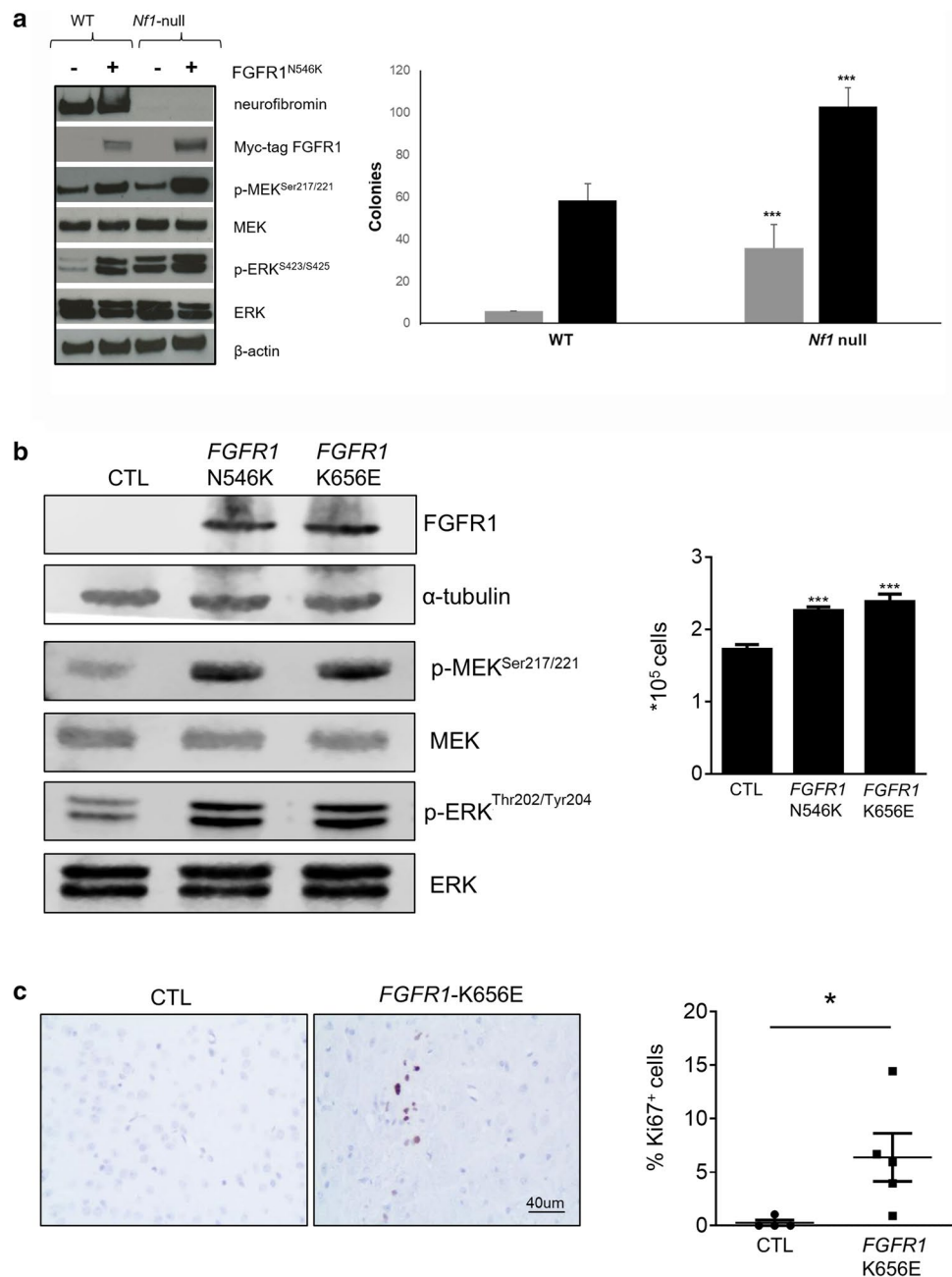


**Fig. 2 a** Oncoplot revealing the spectrum of mutations and clinical parameters across the core clinical cohort. **b** Oncoplot of an additional cohort of 22 samples with incomplete clinical annotation. *amp* amplification, *CN-LOH* copy number loss of heterozygosity, *DNA seq* DNA sequencing, *Dx* diagnosis, *HGAP* high-grade astrocytoma with piloid features, *LGG* low-grade glioma, *LGGNT* low-grade glioma and glioneuronal tumor, *LOH* loss of heterozygosity, *NOS* not otherwise specified, *PA* pilocytic astrocytoma, *PXA* pleomorphic xanthoastrocytoma, *RGNT* rosette-forming glioneuronal tumor, *RNA seq* RNA sequencing. **c** Methylation clustering analysis reveals that the majority of NF1-LGGs group with sporadic pilocytic astrocytomas (PAs)

while the overall survival of subjects in this cohort was excellent (~98%), 52% of children required chemotherapy, over half of which required more than one chemotherapeutic agent. While patients with clinical/radiographic progression may be more likely to undergo biopsy, this high degree of progression and treatment resistance is consistent with a prior report examining non-optic pathway gliomas [7].

These data also raise important implications regarding the incorporation of biopsy into management of presumed LGG in NF1. Given the overall low occurrence of non-NF1

**Fig. 3 a** *Nf1*-null NIH-3T3 cells expressing either empty vector control or mutant *FGFR1*<sup>N546K</sup> were serum starved for 24 h, and lysates immunoblotted with the indicated antibodies. Stable *FGFR1*<sup>N546K</sup> expression results in increased phosphorylated MEK and ERK (left panel), as well as increased colony formation (right panel). Gray bars, vector; Black bars, mutant *FGFR1*<sup>N546K</sup>. \*\*\**P* < 0.05. **b** Transduction of mutant *FGFR1* (N546K, K656E) results in ectopic *FGFR1* expression and increased MEK (Ser<sup>217/221</sup>) and ERK (Ser<sup>423/425</sup>) activation (left panel), and cell growth quantitated by direct cell counting (right panel) relative to empty vector-transduced (CTL) *Nf1*-deficient o-GSCs. **c** Injection of *FGFR1*<sup>K656E</sup>-expressing, but not empty vector-transduced, o-GSCs into the brainstem of wild-type mice reveals glioma-like lesion formation, as evidenced by increased Ki67 labeling (% Ki67<sup>+</sup> cells), 6 months later (upper panel, representative immunohistochemistry; lower panel, quantitation). Scale bar, 40  $\mu$ m. \**P* < 0.05, \*\*\**P* < 0.01



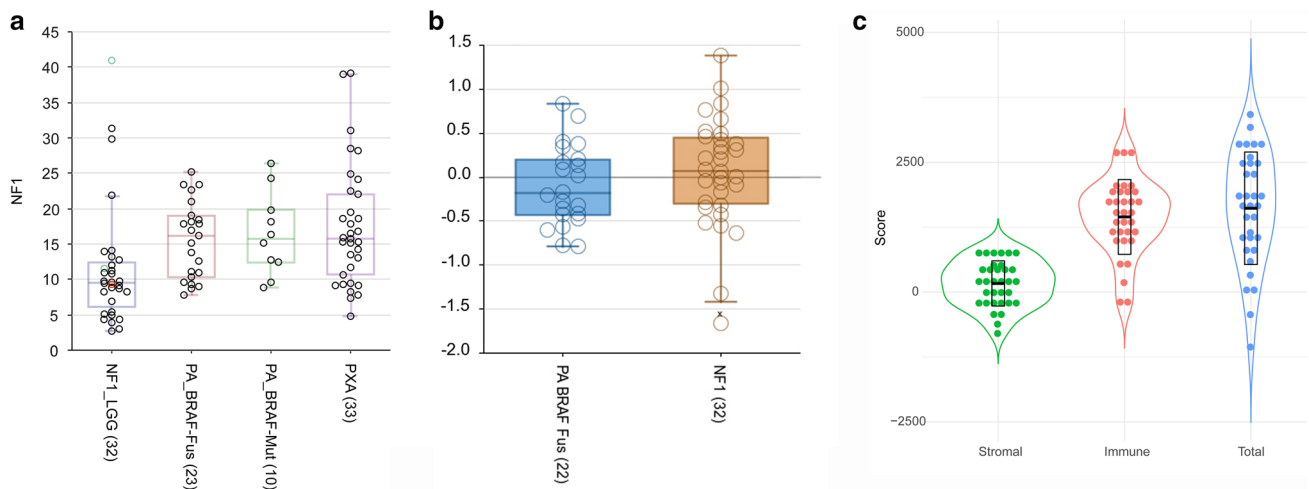


**Fig. 4** **a** NF1-LGGs (LGG\_NF1) have lower *NF1* expression than sporadic PAs (pilocytic astrocytoma with fusion BRAF, PA\_BRAF-fused; pilocytic astrocytoma with mutant BRAF, PA\_BRAF-mut; pleomorphic xanthoastrocytoma, PXA) by RNA sequencing. Of the three samples with RNA sequencing data, but without a detectable second *NF1* mutation, two have *NF1* RNA expression levels similar to those with bi-allelic *NF1* loss (SYN\_NF\_037 with additional *FGFR1* and *PIK3CA* mutations and SYN\_NF\_043 with no additional mutations), while one has elevated *NF1* expression (SYN\_NF\_113

with additional *FGFR1* and *PIK3CA* mutations). SYN\_NF\_037 and SYN\_NF\_113 are noted in green; SYN\_NF\_043 is noted in red. **b** Calculation of the mitogen-activated protein kinase (MAPK) pathway activation scores (MPAS) for NF1-LGGs (NF1; 32 tumors) and a control group of *KIAA1549:BRAF* pilocytic astrocytomas (PA BRAF Fus; 22 tumors), demonstrating no significant difference between groups. **c** RNA sequence analysis demonstrates an increased immune cell component in NF1-LGGs (ESTIMATE violin plots)

mutations or a non-PA methylation class in this cohort of biopsied tumors (which would be likely even lower if all NF1-LGG were biopsied), routine clinical biopsy of typically-appearing LGG in patients with NF1 may not be indicated. In particular, for those with OPHG, the yield of finding an additional actionable mutation is quite low. Although the data do not reveal a significant difference, there appears to be a higher likelihood of finding an additional mutation or non-PA methylation class for those patients with tumors outside of the optic pathway or hypothalamus, raising the question of whether biopsy should be considered for non-OPHG tumors that are refractory to conventional treatment. Other potential indications for biopsy in non-OPHG tumors may include a rapidly growing tumor on neuroimaging, evidence

of peritumoral edema, or the acute development of neurologic signs or symptoms. As treatment strategies for various non-PA LGG evolve, and specific agents are developed for the non-*NF1* mutations identified in this cohort, the rationale for biopsy of NF1-LGG may become stronger. To that end, while yet to be clinically proven, based on the in vitro and in vivo mouse data, the co-occurrence of *FGFR1* mutations in NF1-LGG is functionally significant. As we now enter into a precision oncology era, especially in light of the use of MEK inhibitors for NF1-LGG, future studies will have to determine if LGG with additional non-*NF1* mutations would benefit from the use of molecularly targeted agents or combination treatment strategies.

**Table 2** Differences by tumor location

	Brainstem/midline N=7	Cerebellar/PF NOS N=10	Cortex N=17	OPHG N=13	P value
Age at Biopsy (years)					0.0186
Mean	11.4	11.7	10.1	6	
Median (range)	11.7 (3.7–15.7)	8.2 (4.9–18.9)	7.8 (2.7–17.8)	2.8 (1.9–16.8)	
Length of follow-up (years)					0.9635
Mean	3.5	11.7	10.1	6.2	
Median (range)	4 (0.1–9.3)	2.9 (0.1–19.3)	3.5 (0.6–8.9)	3.8 (0.3–10.2)	
Clinical variable	Number (%)	Number (%)	Number (%)	Number (%)	
Sex					0.6272
Female	4 (57%)	4 (40%)	10 (59%)	5 (38%)	
Male	3 (43%)	6 (60%)	7 (41%)	8 (61%)	
Treatment					0.9799
No	3 (43%)	3 (30%)	6 (35%)	6 (46%)	
Yes	4 (57%)	5 (50%)	9 (53%)	7 (54%)	
Unknown	0 (0%)	2 (20%)	2 (12%)	0 (0%)	
Histology					0.6230
LGG—PA	5 (71%)	4 (40%)	8 (47%)	10 (77%)	
LGG—PA (PMA)	0 (0%)	1 (10%)	1 (6%)	1 (8%)	
LGG—PA with atypical features	0 (0%)	2 (20%)	1 (6%)	0 (0%)	
LGG—grade 2 (DA)	0 (0%)	1 (10%)	3 (18%)	1 (8%)	
LGG—grade 2 (OA)	0 (0%)	0 (0%)	1 (6%)	0 (0%)	
LGG—grade 2 (PXA)	0 (0%)	0 (0%)	1 (6%)	0 (0%)	
LGG—NOS	1 (14%)	2 (20%)	2 (12%)	1 (8%)	
Brain tumor—NOS	1 (14%)	0 (0%)	0 (0%)	0 (0%)	
Methylation subtype					0.2224
PA	5 (71%)	8 (80%)	13 (76%)	12 (92%)	
APA	1 (14%)	0 (0%)	0 (0%)	0 (0%)	
LGGNT	0 (0%)	0 (0%)	2 (12%)	0 (0%)	
MYB	0 (0%)	0 (0%)	2 (12%)	0 (0%)	
RGNT	0 (0%)	1 (10%)	0 (0%)	0 (0%)	
N/A	1 (14%)	1 (10%)	0 (0%)	1 (8%)	
Other mutation					0.6724
No	6 (86%)	8 (80%)	16 (94%)	12 (92%)	
Yes	1 (14%)	2 (20%)	1 (6%)	1 (8%)	
Clinical status					0.1534
Alive	6 (86%)	9 (90%)	14 (82%)	13 (100%)	
Deceased	1 (14%)	0 (0%)	0 (0%)	0 (0%)	
Lost to follow-up	0 (0%)	1 (10%)	3 (18%)	0 (0%)	

Excludes ventricle

APA anaplastic pilocytic astrocytoma, DA diffuse astrocytoma, LGG low-grade glioma, LGGNT low-grade glioma and glioneuronal tumor, MYB MYB methylation group, N/A not available, NOS not otherwise specified, OA oligoastrocytoma, OPHG optic pathway/hypothalamic glioma, PA pilocytic astrocytoma, PF posterior fossa, PMA pilomyxoid astrocytoma, PXA, pleomorphic xanthoastrocytoma, RGNT rosette-forming glioneuronal tumor

**Supplementary Information** The online version contains supplementary material available at <https://doi.org/10.1007/s00401-021-02276-5>.

**Acknowledgements** Research support for this study was provided by a Children's Tumor Foundation Synodos Low Grade Glioma Grant

(2015-18-004 to Michael Fisher, David Gutmann, Stefan Pfister, Joanna Phillips, Angela Waanders). We thank Vidya Browder, Salvo La Rosa and Annette Bakker of the Children's Tumor Foundation for coordinating the efforts of the Synodos Low Grade Glioma and providing input. We thank SAGE Bionetworks for creating the database and housing the data for this study. This research was conducted using samples

made available by The Children's Brain Tumor Network (formerly the Children's Brain Tumor Tissue Consortium). Additional support for other biorepositories were made possible by the UCSF Brain Tumor SPORE Biorepository NIH/NCI P50CA097257, St. Louis Children's Hospital Foundation and Children's Surgical Sciences Institute, and the Morgan Adams Foundation. We thank Jaishri Blakeley (Johns Hopkins University), David Ellison (St. Jude Children's Research Hospital), Mathias Karajannis (Memorial Sloan Kettering Cancer Center), Laura Klesse (University of Texas Southwestern Medical Center), Jeff Knipstein (Children's Hospital of Wisconsin), Nathan Robison (Children's Hospital Los Angeles), Fausto Rodriguez (Johns Hopkins University), Anat Stemmer-Rachamimov (Massachusetts General Hospital), Uri Tabori (Hospital for Sick Children, Toronto), and Lauren Weintraub (Albany Medical Center) for providing specimens that were not used as part of this manuscript. We thank Thomas de Raedt, Till Milde, and Olaf Witt for helpful input.

**Author contributions** MJF and DHG conceptualized and designed the study and analyzed the clinical data. SMP and DTWJ performed the molecular analyses and provided input into study design and overall analyses. XG and PSS performed the in vitro and in vivo mouse model experiments. YL performed the statistical analyses. AJW, JJP, WAW, ACR, and SG are funded members of the Synodos LGG Team, were involved in data and sample acquisition, and provided input into study design and analysis. AG, DK, NKF, AK, MR, LM, SG, MWK, ZW, MF, MS, IO, and SH provided clinical samples and data. SJM created the majority of the tables. All authors had final approval of manuscript.

## Compliance with ethical standards

**Conflict of interest** The authors have no relevant conflicts to disclose.

## References

- Anastasaki C, Morris SM, Gao F, Gutmann DH (2017) Children with 5'-end *NF1* gene mutations are more likely to have glioma. *Neurol Genet* 3:192
- Bandopadhyay P, Ramkissoon LA, Jain P, Bergthold G, Wala J, Zeid R et al (2016) MYB-QKI rearrangements in angiocentric glioma drive tumorigenicity through a tripartite mechanism. *Nat Genet* 48:273–282
- Capper D, Jones DTW, Sill M, Hovestadt V, Schrimpf D, Sturm D et al (2018) DNA methylation-based classification of central nervous system tumours. *Nature* 555:469–474
- Chen YH, McGowan LD, Cimino PJ, Dahiya S, Leonard JR, Lee DY et al (2015) Mouse low-grade gliomas contain cancer stem cells with unique molecular and functional properties. *Cell Rep* 10:1899–1912
- Dobin A, Davis CA, Schlesinger F, Drenkow J, Zaleski C, Jha S et al (2013) STAR: ultrafast universal RNA-seq aligner. *Bioinform (Oxf, Engl)* 29:15–21
- Fontebasso AM, Shirinian M, Khuong-Quang DA, Bechet D, Gayden T, Kool M et al (2015) Non-random aneuploidy specifies subgroups of pilocytic astrocytoma and correlates with older age. *Oncotarget* 6:31844–31856
- Griffith JL, Morris SM, Mahdi J, Goyal MS, Hershey T, Gutmann DH (2018) Increased prevalence of brain tumors classified as T2 hyperintensities in neurofibromatosis 1. *Neurol Clin Pract* 8:283–291
- Gröbner SN, Worst BC, Weischenfeldt J, Buchalter I, Kleinheinz K, Rudneva VA et al (2018) The landscape of genomic alterations across childhood cancers. *Nature* 555:321–327
- Guillermo JS, Creange A, Kalifa C, Grill J, Rodriguez D, Doz F et al (2003) Prognostic factors of CNS tumours in neurofibromatosis 1 (NF1): a retrospective study of 104 patients. *Brain* 126:152–160
- Gutmann DH, McLellan MD, Hussain I, Wallis JW, Fulton LL, Fulton RS et al (2013) Somatic neurofibromatosis type 1 (NF1) inactivation characterizes NF1-associated pilocytic astrocytoma. *Genome Res* 23:431–439
- Jones DT, Jager N, Kool M, Zichner T, Hutter B, Sultan M et al (2012) Dissecting the genomic complexity underlying medulloblastoma. *Nature* 488:100–105
- Jones DT, Hutter B, Jager N, Korshunov A, Kool M, Warnatz HJ et al (2013) Recurrent somatic alterations of *FGFR1* and *NTRK2* in pilocytic astrocytoma. *Nat Genet* 45:927–932
- Lake JA, Donson AM, Prince E, Davies KD, Nellan A, Green AL et al (2020) Targeted fusion analysis can aid in the classification and treatment of pediatric glioma, ependymoma, and glioneuronal tumors. *Pediatr Blood Cancer* 67:e28028
- Li H, Handsaker B, Wysoker A, Fennell T, Ruan J, Homer N, 1000 Genome Project Data Processing Subgroup (2009) The sequence alignment/map format and SAMtools. *Bioinform (Oxf, Engl)* 25:2078–2079
- Liao Y, Smyth GK, Shi W (2014) Feature Counts: an efficient general purpose program for assigning sequence reads to genomic features. *Bioinform (Oxf, Engl)* 30:923–930
- Mahdi J, Shah AC, Sato A, Morris SM, McKinstry RC, Listernick R et al (2017) A multi-institutional study of brainstem gliomas in children with neurofibromatosis type 1. *Neurology* 88:1584–1589
- Mahdi J, Goyal MS, Griffith J, Morris SM, Gutmann DH (2020) Nonoptic pathway tumors in children with neurofibromatosis type 1. *Neurology* 95:e1052–e1059
- Neurofibromatosis Conference statement (1988) National institutes of health consensus development conference. *Arch Neurol* 45:575–578
- Packer RJ, Iavarone A, Jones DTW, Blakeley JO, Bouffet E, Fisher MJ et al (2020) Implications of new understandings of gliomas in children and adults with NF1: report of a consensus conference. *Neuro Oncol* 2:773–784
- Pan Y, Xiong M, Chen R, Ma Y, Corman C, Maricos M et al (2018) Athymic mice reveal a requirement for T-cell-microglia interactions in establishing a microenvironment supportive of Nf1 low-grade glioma growth. *Genes Dev* 32:491–496
- Qaddoumi I, Orisme W, Wen J, Santiago T, Gupta K, Dalton JD et al (2016) Genetic alterations in uncommon low-grade neuroepithelial tumors: BRAF, FGFR1, and MYB mutations occur at high frequency and align with morphology. *Acta Neuropathol* 131:833–845
- Reinhardt A, Stichel D, Schrimpf D, Sahm F, Korshunov A, Reuss DE et al (2018) Anaplastic astrocytoma with piloid features, a novel molecular class of IDH wildtype glioma with recurrent MAPK pathway, CDKN2A/B and ATRX alterations. *Acta Neuropathol* 136:273–291
- Rimmer A, Phan H, Mathieson I, Iqbal Z, Twigg SRF, WGS500 Consortium et al (2014) Integrating mapping-, assembly- and haplotype-based approaches for calling variants in clinical sequencing applications. *Nat Genet* 46:912–918
- Sahm F, Schrimpf D, Jones DT, Meyer J, Kratz A, Reuss D et al (2016) Next-generation sequencing in routine brain tumor diagnostics enables an integrated diagnosis and identifies actionable targets. *Acta Neuropathol* 131:903–910

25. Stein LD, Knoppers BM, Campbell P, Getz G, Korbel JO (2015) Data analysis: create a cloud commons. *Nature* 523:149–151
26. Usta D, Sigaud R, Buhl JL, Selt F, Marquardt V, Pauck D et al (2020) A cell-based MAPK reporter assay reveals synergistic MAPK pathway activity suppression by MAPK inhibitor combination in BRAF-driven pediatric low-grade glioma cells. *Mol Cancer Ther* 19:1736–1750
27. Wagle MC, Kirouac D, Klijn C, Liu B, Mahajan S, Juntala M et al (2018) A transcriptional MAPK pathway activity score (MPAS) is a clinically relevant biomarker in multiple cancer types. *NPJ Precis Oncol* 2:7
28. Wang K, Li M, Hakonarson H (2010) ANNOVAR: functional annotation of genetic variants from high-throughput sequencing data. *Nucleic Acids Res* 38:e164
29. Wefers AK, Stichel D, Schrimpf D, Coras R, Pages M, Tauziede-Espariat A et al (2020) Isomorphic diffuse glioma is a morphologically and molecularly distinct tumour entity with recurrent gene fusions of MYBL1 or MYB and a benign disease course. *Acta Neuropathol* 139:193–209
30. Wong WH, Junck L, Druley TE, Gutmann DH (2019) NF1 glioblastoma clonal profiling reveals KMT2B mutations as potential somatic oncogenic events. *Neurology* 93:1067–1069
31. Worst BC, van Tilburg CM, Balasubramanian GP, Fiesel P, Witt R, Freitag A et al (2016) Next-generation personalised medicine for high-risk paediatric cancer patients—the INFORM pilot study. *Eur J Cancer* 65:91–101
32. Yoshihara K, Shahmoradgoli M, Martinez E, Vegesna R, Kim H, Torres-Garcia W (2013) Inferring tumour purity and stromal and immune cell admixture from expression data. *Nat Commun* 4:2612

**Publisher's Note** Springer Nature remains neutral with regard to jurisdictional claims in published maps and institutional affiliations.

## Authors and Affiliations

Michael J. Fisher<sup>1</sup> · David T. W. Jones<sup>2,3</sup> · Yimei Li<sup>4</sup> · Xiaofan Guo<sup>5</sup> · Poonam S. Sonawane<sup>6</sup> · Angela J. Waanders<sup>1,23</sup> · Joanna J. Phillips<sup>7</sup> · William A. Weiss<sup>8</sup> · Adam C. Resnick<sup>6</sup> · Sara Gosline<sup>9,24</sup> · Jineta Banerjee<sup>9</sup> · Justin Guinney<sup>9</sup> · Astrid Gnekow<sup>10</sup> · Daniela Kandels<sup>10</sup> · Nicholas K. Foreman<sup>11</sup> · Andrey Korshunov<sup>12</sup> · Marina Ryzhova<sup>13</sup> · Luca Massimi<sup>14,28</sup> · Sri Gururangan<sup>15</sup> · Mark W. Kieran<sup>16,25</sup> · Zhihong Wang<sup>17,26</sup> · Maryam Fouladi<sup>18,27</sup> · Mariko Sato<sup>19</sup> · Ingrid Øra<sup>20</sup> · Stefan Holm<sup>21</sup> · Stephen J. Markham<sup>1</sup> · Pengbo Beck<sup>2,3</sup> · Natalie Jäger<sup>2,3</sup> · Andrea Wittmann<sup>2</sup> · Alexander C. Sommerkamp<sup>2,3</sup> · Felix Sahn<sup>12</sup> · Stefan M. Pfister<sup>2,3,22</sup> · David H. Gutmann<sup>5</sup> 

<sup>1</sup> Division of Oncology, The Children's Hospital of Philadelphia, 3615 Civic Center Blvd, Philadelphia, PA, USA

<sup>2</sup> Hopp Children's Cancer Center Heidelberg (KiTZ), Heidelberg, Germany

<sup>3</sup> Pediatric Glioma Research Group, German Cancer Research Center (DKFZ), Heidelberg, Germany

<sup>4</sup> Department of Biostatistics, Epidemiology, and Informatics, University of Pennsylvania, Philadelphia, PA, USA

<sup>5</sup> Department of Neurology, Washington University School of Medicine, 660 South Euclid Avenue, Box 8111, St. Louis, MO 63110, USA

<sup>6</sup> Division of Neurosurgery, The Children's Hospital of Philadelphia, Philadelphia, PA, USA

<sup>7</sup> Departments of Pathology, University of California, San Francisco, CA, USA

<sup>8</sup> Departments of Neurology, University of California, San Francisco, CA, USA

<sup>9</sup> Sage Bionetworks, Seattle, WA, USA

<sup>10</sup> Faculty of Medicine, University Augsburg, Augsburg, Germany

<sup>11</sup> University of Colorado, Denver, CO, USA

<sup>12</sup> Department of Neuropathology, Heidelberg University, Heidelberg, Germany

<sup>13</sup> Department of Neuropathology, NN Burdenko Neurosurgical Research Centre, Moscow, Russia

<sup>14</sup> Fondazione Policlinico A. Gemelli, IRCCS, Rome, Italy

<sup>15</sup> Department of Neurosurgery, UF Health Shands Hospital, Gainesville, FL, USA

<sup>16</sup> Department of Pediatrics, Dana-Farber Cancer Institute, Boston, MA, USA

<sup>17</sup> Division of Hematology/Oncology, Children's Hospital of Michigan, Detroit, MI, USA

<sup>18</sup> Division of Hematology/Oncology, Cincinnati Children's Hospital Medical Center, Cincinnati, OH, USA

<sup>19</sup> Division of Hematology/Oncology, University of Iowa Stead Family Children's Hospital, Iowa City, IA, USA

<sup>20</sup> Lund University Cancer Center, Lund University, Lund, Sweden

<sup>21</sup> Karolinska University Hospital, Stockholm, Sweden

<sup>22</sup> Department of Pediatric Oncology, Hematology, Immunology and Pulmonology, Heidelberg University Hospital, Heidelberg, Germany

<sup>23</sup> Present Address: Division of Hematology/Oncology, Lurie Children's Hospital of Chicago, Chicago, IL, USA

<sup>24</sup> Present Address: Pacific Northwest National Laboratory, Seattle, WA, USA

<sup>25</sup> Present Address: Bristol Myers Squibb, Lawrenceville, NJ, USA

<sup>26</sup> Present Address: Division of Hematology and Oncology, Children's Hospital of Richmond, Richmond, VA, USA

<sup>27</sup> Present Address: Division of Hematology and Oncology, Nationwide Children's Hospital, Columbus, OH, USA

<sup>28</sup> Present Address: Pediatric Neurosurgery, A. Gemelli Hospital, Rome, Italy